UAB
Universitat Autònoma de Barcelona

Dipòsit digital de documents de la UAB

This is the **accepted version** of the journal article:

Gimbert-Suriñach, Carolina [et al.]. «Structural and spectroscopic characterization of reaction intermediates involved in a dinuclear Co-Hbpp water oxidation catalyst». *Journal of the American Chemical Society*, Vol. 138, Num. 47 (November 2016), p. 15291-15294 DOI 10.1021/jacs.6b08532

This version is available at https://ddd.uab.cat/record/338004

under the terms of the IN COPYRIGHT license.

"This document is the Accepted Manuscript version of a Published Work that appeared in final form in Journal of the American Chemical Society, copyright © American Chemical Society after peer review and technical editing by the publisher. To access the final edited and published work see [insert ACS Articles on Request author- directed link to Published Work, see http://pubs.acs.org/doi/abs/10.1021/jacs.6b08532

Structural and Spectroscopic Characterization of Reaction Intermediates Involved in a Dinuclear Co-Hbpp Water Oxidation Catalyst.

Carolina Gimbert-Suriñach,[1] Dooshaye Moonshiram,[2] Laia Francàs,[1] Nora Planas,[3] Varinia Bernales,[3] Fernando Bozoglian,[1] Alexander Guda,[4] Lorenzo Mognon,[1] Isidoro López,[1] Md Asmaul Hoque,[1] Laura Gagliardi,[3] Christopher J. Cramer*[,3] and Antoni Llobet*[,1,5]

[1] Institute of Chemical Research of Catalonia (ICIQ), Barcelona Institute of Science and Technology (BIST), Av. Països Catalans 16, 43007 Tarragona, Spain.

[2] Chemical Sciences and Engineering Division, Argonne National Laboratory, 9700 S. Cass Avenue, Lemont IL 60439, U.S.A.

[3] Department of Chemistry, Supercomputing Institute and Chemical Theory Center, University of Minnesota, 207 Pleasant St. SE, Minneapolis, MN, U.S.A.

[4] International Research Center "Smart Materials", Southern Federal University, 344090 Rostov-on-Don, Russia.

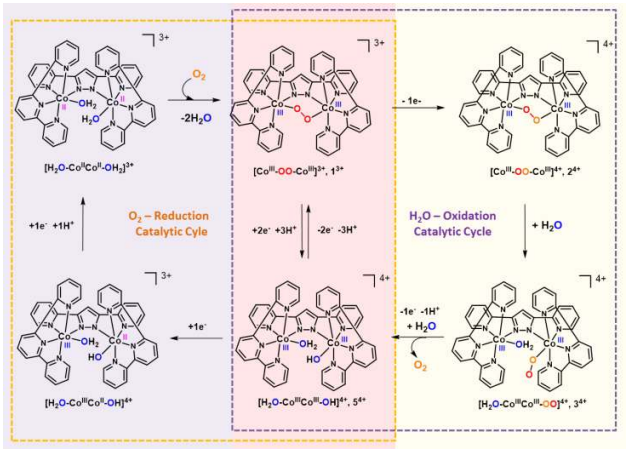
[5] Departament de Química, Universitat Autònoma de Barcelona, 08193 Cerdanyola del Vallès, Barcelona, Spain.

Supporting Information Placeholder

ABSTRACT: An end-on superoxido complex with formula $\{[Co^{III}(OH_2)(trpy)][Co^{III}(OO\cdot)(trpy)](\mu\text{-bpp})\}^{4+}$, $\mathbf{3}^{4+}$, (bpp^- is bis-2-pyridyl-3,5-pyrazolate; trpy is 2,2';6':2"-terpyridine) has been characterized by resonance Raman, electron paramagnetic resonance and x-ray absorption spectroscopies. These results together with on-line mass spectrometry experiments using ^{17}O and ^{18}O isotopically labeled compounds prove that this compound is a key intermediate of the water oxidation reaction catalyzed by the peroxido bridging complex $\{[Co^{III}(trpy)]_2(\mu\text{-bpp})(\mu\text{-OO})\}^{3+}$, $\mathbf{1}^{3+}$. Density Functional Theory calculations agree and complement the experimental data, and offer a complete description of the transition states and intermediates involved in the catalytic cycle.

Oxygen activation by first-row transition metal complexes in low oxidation states has been a very active field of research for the last two decades.[1] A plethora of transition metal peroxido and superoxido complexes in different coordination modes have been prepared and characterized with spectroscopic techniques and even via single-crystal X-ray diffraction in selected instances.[2] The reverse reaction, the oxidation of water to molecular oxygen assisted by first row-transition metal complexes is a field that has emerged recently and the proper characterization of the potential peroxido and/or superoxido reaction intermediates is practically nonexistent.[3] The characterization of such intermediates is hampered by the lability of the metal-ligand bonds that can undergo substitution by water solvent molecules and by the relatively low temperature range at which the reaction can be operated. In sharp contrast, the inverse reaction i.e. the oxygen activation can be carried out in organic solvents and at very low temperatures. Additionally, for the water oxidation reaction, in a number of cases, a competing and/or preferential ligand oxidation occurs[4] which prevents extraction of reliable and meaningful information. In previous work, we have reported the synthesis and X-ray structure of the dinuclear μ-peroxido complex $\{[Co^{III}(trpy)]_2(\mu\text{-bpp})(\mu\text{-OO})\}^{3+}$, denoted as $\mathbf{1}^{3+}$ or $[Co^{III}\text{-OO-}Co^{III}]^{3+}$ hereafter, (trpy is 2,2';6':2"-terpyridine; bpp^- is the bis-2-pyridyl-3,5-pyrazolate) that behaves as powerful catalyst for the $4e^-$ reduction of dioxygen to water.[5] The key structures are depicted in Scheme 1. Further, we have electrochemically characterized the properties of $\mathbf{1}^{3+}$ and have shown by voltammetric and potentiometric techniques its capacity to act as a catalyst for the $4e^-$ oxidation of water to dioxygen.[6]

Scheme 1. Simplified Oxygen Reduction (left) and Water Oxidation (right) catalytic cycles based on the Co-Hbpp complex. In the center (red shadow) the intermediates shared by the two catalytic cycles, $[Co^{III}\text{-OO-}Co^{III}]^{3+}$ ($\mathbf{1}^{3+}$) and $[H_2O\text{-}Co^{III}Co^{III}\text{-OH}]^{4+}$ ($\mathbf{5}^{4+}$).



In this work, we present the preparation of a dinuclear Co superoxido end-on complex, denoted as $\mathbf{3}^{4+}$ or $[H_2O\text{-}Co^{III}Co^{III}\text{-}OO^{\cdot}]^{4+}$, and its thorough characterization based on vibrational, X-ray absorption near edge structure (XANES), Extended X-ray absorption fine structure (EXAFS), Electron Paramagnetic Resonance (EPR) spectroscopies, and by density functional theory, DFT, calculations. In addition, we show for the first time that sequential oxidation of the peroxido derivative, $\mathbf{1}^{3+}$, leads to the just mentioned superoxido $\mathbf{3}^{4+}$, and that further oxidation of the latter generates dioxygen. These two reactions have been carried out using ^{16}O, ^{17}O and ^{18}O labeled complexes to monitor them and to properly characterize potential intermediates. In addition, a coherent mechanistic description of the catalytic cycle is presented based on DFT calculations that agree with the available experimental data.

The dinuclear Co μ-peroxido complex $\mathbf{1}^{3+}$ is prepared in good yields following literature procedures by reacting $\{[Co^{II}(OH_2)(trpy)]_2(\mu\text{-bpp})\}^{3+}$ or its chlorido bridge derivative with molecular dioxygen (Scheme 1).[5] Using dioxygen labeled with different isotopes (^{16}O, ^{17}O or ^{18}O), we have prepared the peroxido complexes $\mathbf{1(32)}^{3+}$ $[Co^{III}\text{-}^{16}O^{16}O\text{-}Co^{III}]^{3+}$, $\mathbf{1(34)}^{3+}$ $[Co^{III}\text{-}^{17}O^{17}O\text{-}Co^{III}]^{3+}$, and $\mathbf{1(36)}^{3+}$ $[Co^{III}\text{-}^{18}O^{18}O\text{-}Co^{III}]^{3+}$, respectively. Figure 1 (left) shows the resonance Raman (rR) spectra obtained for the $\mathbf{1}^{3+}$ set of complexes with the different labeling. A prominent vibration appears at 839 cm^{-1} for $\mathbf{1(32)}^{3+}$ associated with the O-O bond stretching mode. This vibrational transition shifts to 814 cm^{-1} for $\mathbf{1(34)}^{3+}$ and to 795 cm^{-1} for $\mathbf{1(36)}^{3+}$ as expected for a quantum mechanical harmonic oscillator having such changes in reduced mass. For the case of the $\mathbf{1(36)}^{3+}$, rR spectroscopy shows the presence of two bands at 839 and 795 cm^{-1} of similar intensity that are due to a 1:1 ratio of $\mathbf{1(32)}^{3+}$ and $\mathbf{1(36)}^{3+}$ since the dioxygen used in the synthesis contained a 1:1 mixture of $^{36}O_2$:$^{32}O_2$ (See Experimental Section in SI). Similarly, the ^{17}O labeling experiment that used a 9:1 mixture $^{34}O_2$:$^{32}O_2$ of dioxygen, shows a small shoulder at 839 cm^{-1} in the corresponding rR spectrum.

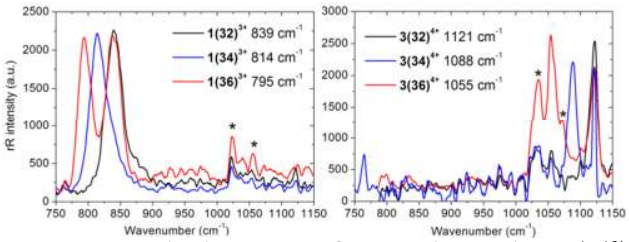
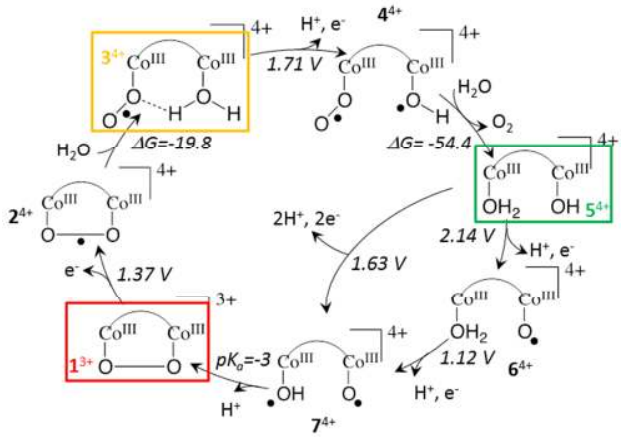


Figure 1. Normalized rR spectra for peroxido complexes $\mathbf{1(32)}^{3+}$ (black line), $\mathbf{1(34)}^{3+}$ (blue line) and $\mathbf{1(36)}^{3+}$ (red line) (Left) and superoxido complexes $\mathbf{3(32)}^{4+}$ (black line), $\mathbf{3(34)}^{4+}$ (blue line) and $\mathbf{3(36)}^{4+}$ (red line) (Right). λ_{exc}=514 nm. Asterisks: solvent resonances.

Chemically, the addition of 1 equivalent of Ce^{IV} to the peroxido complexes $\mathbf{1}^{3+}$ at pH=1.0 generates the corresponding superoxido complexes $\mathbf{2}^{4+}$ or $[Co^{III}\text{-}O^{\cdot}O\text{-}Co^{III}]^{4+}$ that undergo hydrolysis to yield end-on superoxido complexes $\mathbf{3}^{4+}$ or $[H_2O\text{-}Co^{III}Co^{III}\text{-}OO^{\cdot}]^{4+}$ as suggested by DFT calculations and in agreement with XAS spectroscopy. DFT calculations using the SMD(water)/M11-L/ 6-311G(2f,d) predict that the end-on form $\mathbf{3}^{4+}$ is 19.8 kcal/mol more stable than the bridging one $\mathbf{2}^{4+}$ (Scheme 2). Figure 2 shows the optimized DFT structure for the end-on superoxido complex together with the singly occupied molecular orbital (SOMO). The spin density in this orbital is mainly localized on the superoxido group, which forms a hydrogen bond with the neighboring Co-OH_2 group supporting the peroxide bridge as the main oxidation site. Previous electrochemical experiments showed that the oxidation of the peroxido complex $\mathbf{1}^{3+}$ to the superoxido $\mathbf{3}^{4+}$ is chemically and electrochemically reversible and occurs at $E^{o'}$=1.49 V *vs.* NHE.[6] DFT calculations using again SMD(water)/M11-L/ 6-311G(2f,d) predict a value of 1.37 V *vs.* NHE for this oxidation in good agreement with the experimental value and thus suggests that this level of theory will be useful and sufficiently accurate for modeling other properties of the system.

Scheme 2. Calculated Water Oxidation Catalytic Cycle associated with the Co-Hbpp complex. The arc connecting the two Co centers represents the bpp$^-$ bridging ligand. The trpy ligands are not represented for clarity purposes. Red box: starting material $[Co^{III}\text{-}OO\text{-}Co^{III}]^{3+}$, $\mathbf{1}^{3+}$. Yellow box: hydrated one electron oxidation of the former $[H_2O\text{-}Co^{III}Co^{III}\text{-}OO^{\cdot}]^{3+}$, $\mathbf{3}^{4+}$. Green box: $[H_2O\text{-}Co^{III}Co^{III}\text{-}OH]^{4+}$, $\mathbf{5}^{4+}$, species formed after oxygen ejection. Potentials are indicated in V *vs.* the NHE reference electrode at pH=2.0 whereas ΔG are reported in kcal/mol.



Vibrational rR spectroscopy was also carried out for the superoxido complexes with the different O_2 isotopologues, and the results are shown in Figure 1 (right). The O-O bond vi-

bration for the $\mathbf{3(32)}^{4+}$ oxidized complex appears at 1121 cm^{-1}, which is consistent with a superoxido group,[7] although experimentally the end-on and side-on isomers are virtually undistinguishable.[7d,8] Furthermore, the labeled complexes shift to 1088 cm^{-1} and 1055 cm^{-1} for $\mathbf{3(34)}^{4+}$ and $\mathbf{3(36)}^{4+}$, respectively, as expected. Here again, the mixture of isomers is clearly observed in the spectra since we use the peroxido complexes mentioned earlier as starting materials. It is worth noting here that the potential use of mixed labeled oxygen atoms would generate one band for the symmetric side-on complex (Co-$O^{16}O^{18}$-Co) and two for the end-on (CoCo-$O^{16}O^{18}$ and CoCo-$O^{18}O^{16}$). However the energy difference for the two bands generated by the latter complex would be too small to be clearly differentiated in the spectrum (theory predicts a shift of 1-3 cm^{-1} for related complexes).[8]

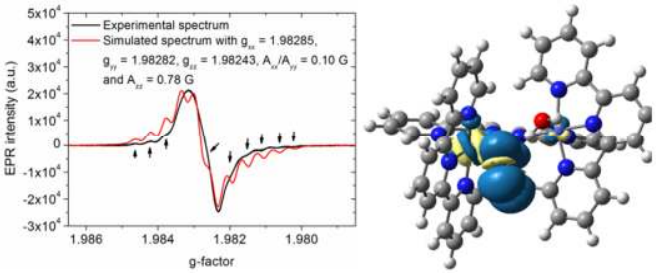


Figure 2. Left, experimental (black line) and simulated (red line) EPR spectrum of $\mathbf{3(34)}^{4+}$. Right, SOMO for the optimized end-on superoxido complex $\mathbf{3(32)}^{4+}$.

The superoxido complexes were also characterized by EPR spectroscopy. For complex $\mathbf{3(32)}^{4+}$ and $\mathbf{3(36)}^{4+}$ a broad band centered at g=1.98 is observed in the EPR spectrum, which is due to the unpaired electron of the superoxido group. The broadness of the peaks is a consequence of the coupling of the superoxido unpaired electron with the nuclear spins of ^{59}Co (I=7/2) that are not well resolved (See Figure S1 in the SI). In sharp contrast, the EPR for $\mathbf{3(34)}^{4+}$ shows a similar spectrum as for $\mathbf{3(32)}^{4+}$ but with a fine structure due to the coupling to the nuclear spin of ^{17}O (I=5/2) as can be observed in Figure 2 together with its mathematical simulation.

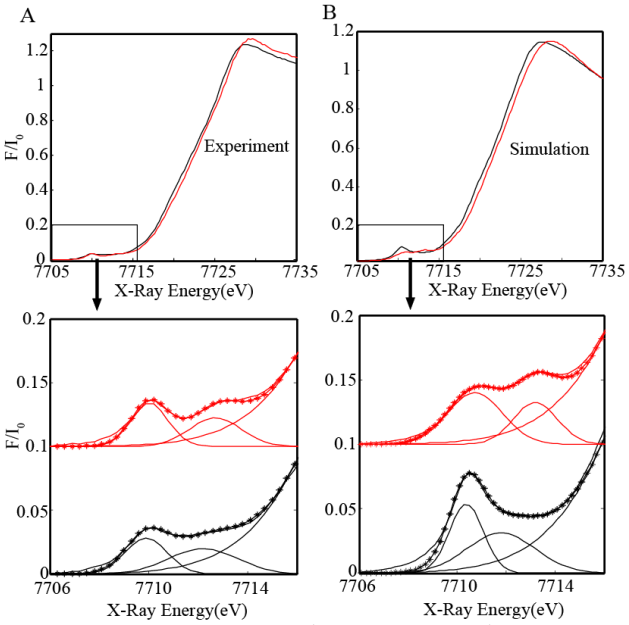


Figure 3. XANES spectra of $\mathbf{1(32)}^{3+}$ (black) and $\mathbf{3(32)}^{4+}$ (red). A) Top: Experimental results. Bottom: Zoom in of Pre-edge regions and Gaussian fits of the 2 pre-edge peaks. B) Top: DFT-MO Simulated data. Bottom: Zoom in of pre-edge region and Gaussian fits of the 2 pre-edge peaks. See also Figure S3 in the Supporting Information.

XANES analysis of the superoxido complex $\mathbf{3}^{4+}$ reveals a small positive shift of the rising edge (0.4 eV) compared to the peroxido $\mathbf{1}^{3+}$ (top left of Figure 3). The shift in energy indicates a change in the electron density and local geometry around the Co metal center and is well reproduced by theoretical XANES simulations shown in Figure 3 (right) thus supporting a peroxido centered oxidation in agreement with rR and EPR results. More interesting is the predominant characteristic multiplet feature in the pre-edge region that distinguishes the superoxido compound from its parent peroxido derivative (Figure 3, bottom). The presence of pre-edge features corresponds to the 1s to 3d quadrupole transitions and dipole excitations of the core electrons into the valence 3d levels hybridized with p orbitals.[9] Upon oxidation with 1 eq. Ce^{IV}, local distortions around the Co center and increased hybridization of the valence 3d states with N/O ligand p-orbitals results in the clear formation of a second pronounced pre-edge feature. As shown by the Gaussian fits in Figure 3 (bottom), the pre-edge region has contribution of two main absorptions centered at *ca.*7709.9 eV and 7712.2 eV for the peroxido derivative. Upon oxidation, the peak at 7712.2 eV slightly shifts to higher energy (7712.7 eV), and becomes more pronounced giving rise to an apparent doublet feature that is not as obvious for the starting peroxido compound (compare black and red traces). Theoretical DFT-MO XANES calculations of the superoxido derivatives $\mathbf{2}^{4+}$ and $\mathbf{3}^{4+}$ in Scheme 2 reproduce well this shift especially for the non-symmetric end-on compound $\mathbf{3}^{4+}$, where the doublet feature is more noticeable (Figure 3 and Figure S3). In addition, EXAFS analysis show a slightly better fit for $\mathbf{3}^{4+}$ (see supporting information). Previous electrochemical experiments revealed that the superoxido complex $\mathbf{3}^{4+}$ can be further oxidized by one electron at 1.80 V *vs.* NHE.[6] M11-L/DFT calculations suggest the formation of a diradical hydroxyl-superoxido species $[HO^{\cdot}\text{-}Co^{III}Co^{III}\text{-}OO^{\cdot}]^{4+}$, $\mathbf{4}^{4+}$, obtained from a PCET process occurring at a potential of 1.71 V *vs.* NHE

(Scheme 2). This new redox couple ($\mathbf{3}^{4+}/\mathbf{4}^{4+}$) is responsible for a large electrocatalytic wave in the 1.8-2.0 V *vs*. NHE potential range associated with catalytic water oxidation to dioxygen.[6] In agreement with these electrochemical results, further addition of Ce^{IV} to the superoxido complexes $\mathbf{3}^{4+}$ should generate dioxygen. Indeed, Figure 4 shows the on-line mass spectrometry (MS) results of adding 4 equivalents of Ce^{IV} to a solution of $\mathbf{1(34)}^{3+}$ that generates a mixture of approximately 10:1 of $^{34}O_2$:$^{32}O_2$ in very good agreement with the expected 9:1 ratio of the starting materials. In a similar manner $\mathbf{3(32)}^{4+}$ and $\mathbf{3(36)}^{4+}$ also give the expected ratios of labeled dioxygen (Figure S8).

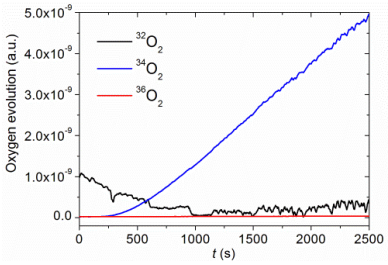


Figure 4. O_2 evolution profile monitored via on-line MS for a mixture containing $\mathbf{1(34)}^{3+}$ and 4 equivalents of $(NH_4)_2Ce(NO_3)_6$ in 0.1 M triflic acid (pH=1.0).

Further DFT calculations were undertaken to complete the catalytic cycle (Scheme 2). Oxygen ejection from $\mathbf{4}^{4+}$ concomitant with solvent coordination generates a dicobalt aqua-hydroxo complex at oxidation state III, $[HO\text{-}Co^{III}Co^{III}\text{-}OH_2]^{4+}$, $\mathbf{5}^{4+}$. Species $\mathbf{5}^{4+}$ is predicted to be further oxidized by a two-electron/two-proton single step at a potential of 1.63 V *vs*. NHE (which is slightly lower than that required for the oxidation of $\mathbf{3}^{4+}$ to $\mathbf{4}^{4+}$) to generate the highly reactive oxyl-hydroxyl species, $[HO^{\cdot}\text{-}Co^{III}Co^{III}\text{-}O^{\cdot}]$, $\mathbf{7}^{4+}$. The aqueous pK_a of $\mathbf{7}^{4+}$ is predicted to be -3, so proton loss is expected to be spontaneous to generate the initial peroxo species $\mathbf{1}^{3+}$. Indeed, it cannot be ruled out that the oxidation of $\mathbf{5}^{4+}$ may occur as an overall two-electron/three-proton step, as we have not attempted to model the specific kinetics of these PCET transformations. The resulting bis[cobalt(III)-oxyl] compound, $\mathbf{7}^{4+}$, is not predicted to be stationary at the M11/L level, but spontaneously forms an O–O bond leading to the bridged peroxido complex $\mathbf{1}^{3+}$, closing the catalytic cycle. Theory indicates that $\mathbf{7}^{4+}$ will have extremely short lifetimes, thereby disfavoring O–O bond formation through nucleophilic attack of water on the oxyl fragment. It is interesting to note here the fundamental role played by the bpp^- ligand in maintaining the two metal centers in close proximity. In the O-O bond formation step, the ligand pre-organizes the two Co-O moieties in $\mathbf{7}^{4+}$ so that the O-O bond formation is entropically favored. Further, the last step before oxygen ejection involves the formation of a diradical hydroxyl-superoxido species $\mathbf{4}^{4+}$, where the Co-O$^{\cdot}$H and the Co-OO$^{\cdot}$H moieties are situated in close proximity. Electron transfer to the cobalt hydroxyl moiety from the superoxido ligand is then ultimately responsible for the oxygen ejection. The need to generate a Co-hydroxyl simultaneously with a Co-superoxido cannot occur at a single-site as would be required in a mononuclear complex. Notice also that the water oxidation reaction cycle involves oxygen only (not metal-centered) redox processes involving the superoxido and the aqua ligands in different protonation states (i.e., oxyl or hydroxyl radicals). The Co^{III} centers act as scaffolds strategically supporting the reactive oxygen radical species but do not undergo metal center redox processes.

Scheme 1 shows the interplay between the oxygen reduction and water oxidation catalytic cycles for the Co-Hbpp complex. The two catalytic cycles share two common reactive intermediates, $[Co^{III}\text{-}OO\text{-}Co^{III}]^{3+}$, $\mathbf{1}^{3+}$, and $[H_2O\text{-}Co^{III}Co^{III}\text{-}OH]^{4+}$, $\mathbf{5}^{4+}$, (shown in the center of Scheme 1, whose X-ray structures have been described previously).[5,6] Oxidation of $[Co^{III}\text{-}OO\text{-}Co^{III}]^{3+}$ leads to the water oxidation cycle (yellow box in Scheme 1) whereas reduction of $[H_2O\text{-}Co^{III}Co^{III}\text{-}OH]^{4+}$ leads to the oxygen reduction cycle (purple box in Scheme 1). The use of similar type of species for O-O bond formation and O-O bond cleavage but at different oxidation states parallels the chemistry that occurs at the chloride dismutase (Chl-D)[10] and Cyt-P450[11] respectively in nature. For Cyt-P450 cycle the Fe(II) porphyrin active center reacts with oxygen to generate an Fe(III)-superoxido species that eventually leads to O-O bond scission forming an Fe^{IV}=O high oxidation state species responsible for organic substrate oxidations. On the other hand, the catalytic cycle proposed for Chl-D, the lowest oxidation state proposed for the Fe porphyrin is "III" at which point molecular oxygen is released.

In conclusion, we report detailed characterization of reaction intermediates involved in the catalytic cycle of a first-row transition-metal-based water-oxidation catalyst. This work is also important because it can be taken as a low molecular weight model of Co oxides,[12a,3b] although it is important to keep in mind that the electronic coupling through the bpp^- ligand can be significantly different from that of oxo-bridged Co oxides. The latter together with Ni oxides are amongst the most active earth abundant water oxidation heterogeneous catalysts.[12a,13] For those oxides, thorough structural characterizations and mechanistic studies of active species are inherently difficult, given their heterogeneous nature. In addition, we also show that the same transition metal complex can be used for both the water oxidation and oxygen reduction catalytic reactions.

ASSOCIATED CONTENT

Supporting Information

Additional spectroscopic and computational details. This material is available free of charge via the Internet at http://pubs.acs.org.

AUTHOR INFORMATION

Corresponding Author

cramer@umn.edu; allobet@iciq.cat;

ACKNOWLEDGMENT

Financial support from MINECO and FEDER (CTQ-2016-80058-R, SEV-2013-0319, and CTQ-2014-52974-REDC) and EU COST actions CM1202 and CM1205. DM thanks U.S. Department of Energy (DOE), Office of Science, Basic Energy Sciences, CSGB Division (contract no. DE-AC02-06CH11357) and resources of the Advanced Photon Source at ANL. Some rR done at the Center of Nanoscale materials at ANL, supported by DOE with same contract no. CJC thanks the U.S. NSF for support (CHE-1361595). LG was partially supported by the U.S. DOE, Office of Basic Energy Sciences, under SciDAC Grant No. DE-SC0008666.

REFERENCES

[1] (a) Hematian, S.; Garcia-Bosch, I.; Karlin, K. D. *Acc. Chem. Res.* **2015**, *48*, 2462-2474. (b) Nam, W. *Acc. Chem. Res.* **2015**, *48*, 2415-2423. (c) Cramer, C. J.; Tolman, W. B. *Acc. Chem. Res.* **2007**, *40*, 601-608. (d) Citek, C.; Herres-Pawlis, S.; Stack, T. D. P. *Acc. Chem. Res.* **2015**, *48*, 2424-2433.

[2] (a) Cho, J.; Jeon, S.; Wilson, S. A.; Liu, L. V.; Kang, E. A.; Braymer, J. J.; Lim, M. H.; Hedman, B.; Hodgson, K. O.; Valentine, J. S.; Solomon, E. I.; Nam, W. *Nature* **2011**, *478*, 502-505. (b) Bukowski, M. R.; Koehntop, K. D.; Stubna, A.; Bominaar, E. L.; Halfen, J. A.; Muenck, E.; Nam, W.; Que, L., Jr. *Science* **2005**, *310*, 1000-1002.

[3] (a) Concepcion, J. J.; Tsai, M.-K.; Muckerman, J. T.; Meyer, T. J. *J. Am. Chem. Soc.* **2010**, *132*, 1545-1557. (b) Zhang, M.; de Respinis, M.; Frei, H. *Nature Chem.* **2014**, *6*, 362-367.

[4] (a) Wang, J.-W.; Ptahik, S.; Lu, T.-B. *ACS Catal.*, **2016**, *6*, 5062-5068. (b) Hoffert, W. A.; Mock, M. T.; Appel, A. M.; Yang, J. Y. *Eur. J. Inorg. Chem.* **2013**, 3846-3857. (c) Radaram, B.; Ivie, J. A.; Singh, W. M.; Grudzien, R. M.; Reibenspies, J. H.; Webster, C. E.; Zhao, X. *Inorg. Chem.* **2011**, 50, 10564-10571.

[5] Fukuzumi, S.; Mandal, S.; Mase, K.; Ohkubo, K.; Park, H.; Benet-Buchholz, J.; Nam, W.; Llobet, A. *J. Am. Chem. Soc.* **2012**, *134*, 9906-9909.

[6] Rigsby, M. L.; Mandal, S.; Nam, W.; Spencer, L. C.; Llobet, A.; Stahl, S. S. *Chem. Sci.* **2012**, 3, 3058-3062.

[7] (a) Barraclough, C. G.; Lawrance, G. A.; Lay, P. A. *Inorg. Chem.* **1978**, *17*, 3317-3322. (b) Schmidt, S.; Heinemann, F. W.; Grohmann, A. *Eur. J. Inorg. Chem.* **2000**, 1657-1667. (c) Rajani, C.; Kincaid, J. R.; Petering, D. H. *J. Am. Chem. Soc.* **2004**, *126*, 3829-3836. (d) Nakamoto, K. Infrared and raman Spectra of Inorganic and Coordination Compounds, 6th Edn., John wiley & Sons Inc., Hoboken, New Jersey, 2009.

[8] (a) Kinsinger, C. R.; Gherman, B. F.; Gagliardi, L.; Cramer, C. J. *J. Biol. Inorg. Chem.* **2005**, *10*, 778-789. (b) Shan, X.; Que, L., Jr. Proc. Natl. Acad. Sci. U. S. A **2005**, *102*, 5340-5345.

[9] (a) Loeb, K. E.; Westre, T. E.; Kappock, T. J.; Mitic, N.; Glasfeld, E.; Caradonna, J. P.; Hedman, B.; Hodgson, K. O.; Solomon, E. I. *J. Am. Chem. Soc.* **1997**, *119*, 1901-1915. (b) Westre, T. E.; Kennepohl, P.; DeWitt, J. G.; Hedman, B.; Hodgson, K. O.; Solomon, E. I. *J. Am. Chem. Soc.* **1997**, *119*, 6297-6314. (c) de Groot, F. *Chem. Rev.* **2001**, *101*, 1779. (d) Chandrasekaran, P.; Stieber, S. C. E.; Collins, T. J.; Que, J. L.; Neese F.; DeBeer, S. *Dalton Trans.* **2011**, *40*, 11070-11079.

[10] (a) Mlynek, G.; Sjöblom, B.; Kostan, J.; Füreder, S.; Maixner, F.; Gysel, K.; Furtmüller, P. G.; Obinger, C.; Wagner, M.; Daims, H.; Djinović-Carugo, K. *J. Bacteriol.* **2011,** *193,* 2408-2417. (b) Sun, S.; Li, Z.-S.; Chen, S.-L. *Dalton Trans.* **2014**, *43*, 973–981.

[11] (a) Ener, M. E.; Lee, Y.-T.; Winkler, J. R.; Gray, H. B.; Cheruzel, L. *PNAS* **2010**, *107*, 18783-18786. (b) Guengerich, F. P. *J. Biochem. Mol. Toxicol.* **2007**, *21*, 163–168.

[12] (a) McCrory, C. C. L.; Jung, S.; Ferrer, I. M.; Chatman, S. M.; Peters, J. C.; Jaramillo, T. F. *J. Am. Chem. Soc.* **2015**, *137*, 4347. (b) Nguyen, A. I.; Ziegler, M. S.; Oña-Burgos, P.; Sturzbecher-Hohne, M.; Kim, W.; Bellone, D. E.; Tilley, T. D. *J. Am. Chem. Soc.* **2015,** *137*, 12865–12872. (c) Coehn, A.; Gläser, M. *Zeit. Anorg. Chem.* **1902**, 33, 9-24.

[13] (a) Hu, S.; Shaner, M. R.; Beardslee, J. A.; Lichterman, M.; Brunschwig, B. S.; Lewis, N. S. *Science*, **2014**, *344*, 1005-1009. (b) Kenney, M. J.; Gong, M.; Li, Y.; Wu, J. Z.; Feng, J.; Lanza, M.; Dai, H. *Science* **2013**, *342*, 836-840.

Table of Contents

